JOURNAL OF GEOPHYSICAL RESEARCH: SPACE PHYSICS, VOL. 118, 6723–6735, doi:10.1002/jgra.50599, 2013

Three-dimensional simulation of dust charging and dusty plasma using SPIS

A. K. Anuar,[1,2] F. Honary,[1] M. Hapgood,[1,3] and J.-F. Roussel[4]

Received 31 July 2012; revised 26 July 2013; accepted 25 September 2013; published 10 October 2013.

[1] This paper presents new observations of the behavior of simulated dust particles in space plasma based on a 3-D particle in cell code. Multistep Monte Carlo collision is employed to simulate the dust charging process, which is validated for the cases of charging of isolated dust particle and ensemble dust particles, where results indicate good agreement between simulation and theories. The code is then used to investigate plasma properties near a charged surface in a vicinity of a cloud of dust particles. The simulation reveals that a cloud of dust particle close to a spacecraft surface affects plasma densities around the spacecraft as well as the spacecraft's surface potential. It is suggested that dust cloud causes the surface to charge to higher negative potential. The simulation also suggests that the combination of surface potential and dust cloud potential produces a region of trapped low-energy electrons.

Citation: Anuar, A. K., F. Honary, M. Hapgood, and J.-F. Roussel (2013), Three-dimensional simulation of dust charging and dusty plasma using SPIS, *J. Geophys. Res. Space Physics*, *118*, 6723–6735, doi:10.1002/jgra.50599.

1. Introduction

[2] Dust particles are ubiquitous in space and Earth's atmosphere and have been a subject of intensive research for decades [see *Shukla*, 2001; *Fortov et al.*, 2005, and references therein]. Interstellar and interplanetary space, planetary rings, comets, and asteroids are examples where dust particles are naturally present [*Spitzer*, 1941; *Mendis*, 1979; *Goertz*, 1989]. They are also found in the vicinity of a spacecraft, a result of material degradation, waste dumping, thrusters firing, or simply by the release of trapped dust particle on the spacecraft surface and have been shown to be the cause of many measurement and operational errors [*Murphy and Chiu*, 1991; *Goree and Chiu*, 1993; *Robinson et al.*, 1991].

[3] These submicron and micron size particles are charged when immersed in plasma, making them respond to electric and magnetic fields and participate in the collective plasma behavior. In addition, the dust's heavier mass means that it has a smaller charge-to-mass ratio (q/m) and is more affected by gravitational force compared to other elementary particles especially in regions close to large planetary bodies. Dust interactions with local plasma population increases the complexity of the plasma system which is why it is sometime referred to as *complex plasma* [see, for example, *Shukla*, 2001; *Fortov et al.*, 2005].

[1]Department of Physics, Lancaster University, Lancaster, UK.
[2]University Tun Hussein Onn Malaysia, Malaysia.
[3]Rutherford Appleton Laboratory, Didcot, UK.
[4]ONERA, Toulouse, France.

Corresponding author: A. K. Anuar, Department of Physics, Lancaster University, Lancaster LA1 4YD, UK. (a.anuar@lancaster.ac.uk)

2169-9380/13/10.1002/jgra.50599

[4] Many efforts have been taken to study the dust-plasma interactions which include using particle-in-cell (PIC) code to simulate the dust electrodynamics [*Birdsall*, 1991] and Monte Carlo collision (MCC) for the dust charging process [*Goree*, 1994; *Lapenta and Brackbill*, 1997; *Rovagnati et al.*, 2007]. This paper presents new observations on the behavior of the simulated dust particles in space plasma based on a three-dimensional particle-in-cell code with Monte Carlo collision (PIC-MCC). The Spacecraft Plasma Interaction System (SPIS) which is publicly available from the SPIS Web site (www.spis.org) [*Hilgers et al.*, 2008; *Roussel et al.*, 2008], and was developed for the purpose of simulating spacecraft charging has been further developed to include dust particle dynamics simulation. The new code (SPIS-dust) incorporates multistep Monte Carlo algorithm [*Gatsonis et al.*, 1994] to simulate the dust particle charging process. The code considers the dust charging process by the ambient plasma and the simulated charging process is compared with the orbital motion limited theory (OML) [*Mott-Smith and Langmuir*, 1926]. The code is then used to study the plasma response in the case of dust cloud with and without the presence of charged surface.

1.1. Dusty Plasma

[5] Dusty plasma loosely refers to fully or partially ionized electrically conducting gases whose constituents are electrons, ions, charged dust grains, and neutrals, where the dust particles of interest are those of the size between tenths of nanometers and few hundreds of a microns. These microscopic dust particles, when immersed in space plasma, start collecting or emitting electrons and ions, thus charging the dust particles to a floating potential where total current entering and leaving the dust surface are balanced.

[6] Physical properties of dust particles such as their size, mass, density, and whether they are positively or negatively

charged vary depending on their origin and surroundings. In this paper, the dust particles are assumed to be spherical with dust radius r_d = 100 μm. This assumption is believed to not affect the generality of the solution as long as the dust radius $r_d \ll \lambda_D$ where λ_D is the plasma shielding length [*Cui and Goree*, 1994]. In typical space dusty plasma environment, the dust radius value can be distributed between a few tenths of nanometers and a few hundreds of micrometers. In this paper the choice of a unique radius value, r_d = 100μm is made to simplify the implementation of the Multistep Monte Carlo collision algorithm. It can be also noted that, r_d = 100μm is typically the value of the maximum permitted size of released microparticle into sensitive instruments in most space mission [*Brieda et al.*, 2010]. Therefore, dusty plasma around spacecraft with released particles of this size may exist. In this paper, only dust charging by ambient plasma is considered.

1.2. Dusty Plasma Characteristics

[7] The term dusty plasma is reserved for the case where interaction between each dust particle in the system exists and the system behaves collectively, as opposed to dust-in-plasma where the dust particle is in isolation. The distinction between both cases depends on the dusty plasma characteristics length which include the dust radius r_d, dust average intergrain distance a, and λ_D. λ_D is given as [*Jana et al.*, 1993; *Shukla*, 1994]

$$\lambda_D^{-2} = \lambda_{D_e}^{-2} + \lambda_{D_i}^{-2} \tag{1}$$

where λ_{D_e} and λ_{D_i} are the electron and proton Debye length given by

$$\lambda_{D_{e,i}} = \sqrt{\varepsilon_0 k T_{e,i} / \left(n_{e,i} e^2\right)} \tag{2}$$

ε_0 is the space permittivity, $T_{e,i}$ is the electron and ion temperature, and $n_{e,i}$ is the electron and ion density, respectively.

[8] The dust is in isolation when $r_d \ll \lambda_D \ll a$. The dust charging process is then similar to the case of a probe immersed in plasma which can be modeled by the Orbital Motion Limited (OML) theory [*Mott-Smith and Langmuir*, 1926]. Whereas, dusty plasma refers to a case where $r_d \ll a \ll \lambda_D$. In this case, dust particles interact with each other and participate in the collective behavior of the plasma. The dust particles could then be assumed to be another plasma species with varying charge number which interact not only among themselves but also with the surrounding plasma.

[9] The dust charge $Q_d = eZ_d$, where Z_d is the absolute charge number, depends mainly on the ambient plasma density, plasma temperature, and dust density. The OML theory gives the current entering and leaving the dust surface by [*Mott-Smith and Langmuir*, 1926]

$$I_s = 4\pi r_d^2 n_{s0} q_s \sqrt{\frac{kT_s}{2\pi m_s}} \left(1 - \frac{q_s \phi_d}{kT_s}\right) \quad \text{for } q_s\phi_d < 0 \tag{3}$$

and

$$I_s = 4\pi r_d^2 n_{s0} q_s \sqrt{\frac{kT_s}{2\pi m_s}} \exp\left(-\frac{q_s \phi_d}{kT_s}\right) \quad \text{for } q_s\phi_d > 0 \tag{4}$$

where s is the plasma species (electron, ion), n_{s0} is the species density at a distance far away from the plasma cloud, q is the species charge, and ϕ_d is the dust surface potential. In addition, emission currents such as photoemission, electron/ion secondary emission and backscattering can be included in the current balance equation given by [*Whipple*, 1981]

$$\sum I_e + I_i + I_{\text{ph}} + I_{\text{sec}} + I_{\text{back}} = 0. \tag{5}$$

Taking only currents due to the ambient plasma and assuming that $T_e \sim T_i$, an isolated dust particle is expected to charge to negative potential because of the higher electrons' thermal velocity compared to ions' thermal velocity. In this case, the particle's surface potential is $-2.51 k_B T_e/e$ for hydrogen plasma and $-3.6 k_B T_e/e$ for oxygen plasma [*Northrop*, 1992].

[10] For nonisolated dust, charging currents in (3) and (4) need to be complimented with the charge neutrality condition which determines average charge on each dust particle. Increase in dust density results in a lower charge number per dust particle as there are more dust particles competing for the same number of plasma particles. *Havnes et al.* [1990] has introduced the parameter P that describes the collective behavior of a dust cloud in space plasmas given by

$$P = 6.95 \times 10^6 T_{\text{eV}} r_d n_d / n_{\text{e0}} \tag{6}$$

where r_d is the dust radius in centimeter and T_{eV} is the plasma temperature in eV. At a low P value, e.g., at $P \ll 1$, the dust particle has been shown to charge to the value similar to an isolated dust particle and plasma quasi-neutrality is a good approximation. However, as P increases, the high number of plasma particles absorption by the dust particles result in a perturbed plasma where the average dust cloud potential approaches 0 V [*Havnes et al.*, 1987, 1990].

1.3. Electrodynamics Model

[11] Motion of plasma species $s = i, e$ are described by the following equations:

$$\begin{aligned} m_s \frac{\mathrm{d}\mathbf{V}_s}{\mathrm{d}t} &= q_s \left(\mathbf{E} + \mathbf{V}_s \times \mathbf{B}\right) + \mathbf{F}_{sj} \\ \frac{\mathrm{d}\mathbf{X}_s}{\mathrm{d}t} &= \mathbf{V}_s \end{aligned} \tag{7}$$

where $\mathbf{V}_s$ is the velocity of species s, m_s is the mass, $\mathbf{X}_s$ is the position, q_s is the charge, $\mathbf{E}$ and $\mathbf{B}$ are the electric and magnetic fields, and $\mathbf{F}_{sj}$ is the force due to collision with other species. A charged dust motion follow the same equation as the plasma species with the addition of multitude of other forces such as the gravitational force ($\mathbf{F}_g$), momentum transfer due to collision with neutrals and ions, Coulomb drag force ($\mathbf{F}_c$) and neutral drag ($\mathbf{F}_n$) given by

$$\begin{aligned} m_d \frac{\mathrm{d}\mathbf{V}_d}{\mathrm{d}t} &= Q_d(t) \left(\mathbf{E} + \mathbf{V}_d \times \mathbf{B}\right) + \mathbf{F}_g + \mathbf{F}_c + \mathbf{F}_n \\ \frac{\mathrm{d}\mathbf{X}_d}{\mathrm{d}t} &= \mathbf{V}_d \end{aligned} \tag{8}$$

where d refers to dust. The dust charge $Q_d(t)$ is a function of time and is given by

$$\frac{\mathrm{d}Q_d}{\mathrm{d}t} = I(t) \tag{9}$$

where $I(t)$ is the total current received by the particulate. The electric field $\mathbf{E} = -\nabla\phi$ is given by Poisson's equation as

$$\nabla^2 \phi(r,t) = -\frac{1}{\epsilon_0} \left(q_i n_i - e n_e - n_d Q_d\right) \tag{10}$$

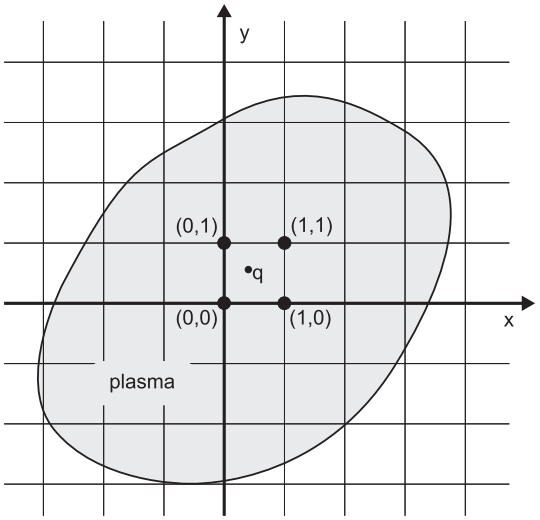

Figure 1. Representation of the mathematical grid used in 2-D PIC modeling [*Birdsall*, 1991]. Superparticles q deposited its *weighted* charge and current densities on the neighboring nodes and on the surface between these nodes. Electric and magnetic fields are obtained from the charge and current density which will then be used to calculate the superparticle motion in the simulation plane [*Birdsall*, 1991].

where n_i, n_e, and n_d are the ion, electron, and dust density, respectively, $q_i = Z_i e$ is the ion charge and Q_d is given for negatively charged dust ($Q_d = -eZ_d$).

[12] The right-hand side term include the charge from all dusty plasma constituents and should reach an equilibrium state when the charge neutrality condition is met, i.e.,

$$q_i n_i = e n_e - Q_d n_d \tag{11}$$

where electron and ion density are given by $n_e = n_{e0}\exp\left(\frac{e\phi_s}{k_B T_e}\right)$, $n_i = n_{i0}\exp\left(-\frac{e\phi_s}{k_B T_e}\right)$ and n_{s0} is the unperturbed number density of the plasma.

2. Simulation

[13] A self consistent dusty plasma simulation requires solving the plasma and dust particle motion (equations (7) and (8)), the dust charging equation (9) and Poisson's equation (10). This is done by dividing the simulation volume into a mathematical grid or *mesh* which overlay all particles in the simulation volume and is known as *particle-in-cell* (PIC) method. Figure 1 shows an example of the mathematical grid often used in a 2-D PIC code which uses equally sized grid to split the simulation plane into small cells with four nodes on each cell. Instead of simulating all particles in the simulation plane or volume, PIC technique simulates *superparticles*. Superparticles represent many particles where their charge and weight (number of particles it represents) are deposited on the nearby nodes and/or mesh surfaces. The net charge densities are used to find electric potential at the nodes (equation (10)) which is then used to solve Maxwell's equation for the fields (**E** and **B**) on the mesh. These fields are then reassigned as forces experienced by the particles in order to solve the motion of plasma and dust particles (equations (7) and (8)).

2.1. PIC-MCC

[14] The interaction between plasma species and the dust particle is simulated via Monte Carlo collision (MCC) algorithm, which is based on the assumption that dust charging is a collisional event that can be modeled using MC fashion. The MCC method had been used extensively to simulate collision between plasma particles with neutrals and has been adopted for multistep dust collision by *Gatsonis et al.* [1994]. Multistep collision allows MCC implementation in highly collisional system and could enable a much larger time step to be used compared to the PIC recommended time step of $0.1\Omega_{p,e}$ [*Birdsall*, 1991], where $\Omega_{p,e}$ is the inverse of electron plasma frequency, i.e., $1/\omega_{p,e}$.

[15] The computational sequence of PIC-MCC is shown in Figure 2. In the PIC-MCC algorithm, an additional step is performed to check for possible collisions between plasma particles and dust particles. In the event of collision, a number of plasma particles are removed from the simulation and their charges are assigned to the corresponding dust particle. This is based on the assumption that all collisions are of absorption type where the colliding plasma particles stick to the dust surface. The whole process is repeated for a specific time period or until the whole system reaches its steady state.

[16] The determination of collision starts with finding the absorption collision frequency, ν_s from

$$\nu_s = n_s \sigma_s v_{\text{rel}} \tag{12}$$

where n_s is the local density of the plasma species in that particular cell, σ_s is the absorption cross section, and v_{rel} is the relative velocity between plasma species and dust particle. Assuming the dust is much heavier than the species, v_{rel} can be estimated to be $\sim v_s$. The dust collision cross section σ_s is calculated based on the following formula given by *Havnes et al.* [1987] as

$$\sigma_s = \pi r_d^2 \left(1 - \frac{\Delta\phi}{1/2 m_s |v_s|^2 / q_s}\right) \tag{13}$$

where r_d is the dust radius, $\Delta\phi$ is the potential difference between the particulate and local plasma, m_s and v_s are the plasma species mass and velocity, respectively, and q_s is the species charge. In the case of an isolated dust ($a > \lambda_D$), $\Delta\phi$

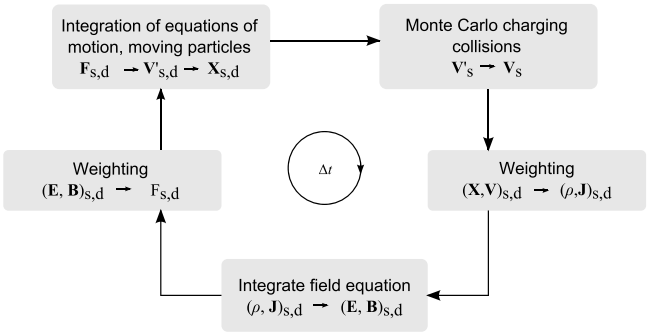

Figure 2. Computational sequence implemented in particle-in-cell code, with the inclusion of Monte Carlo collision algorithm.

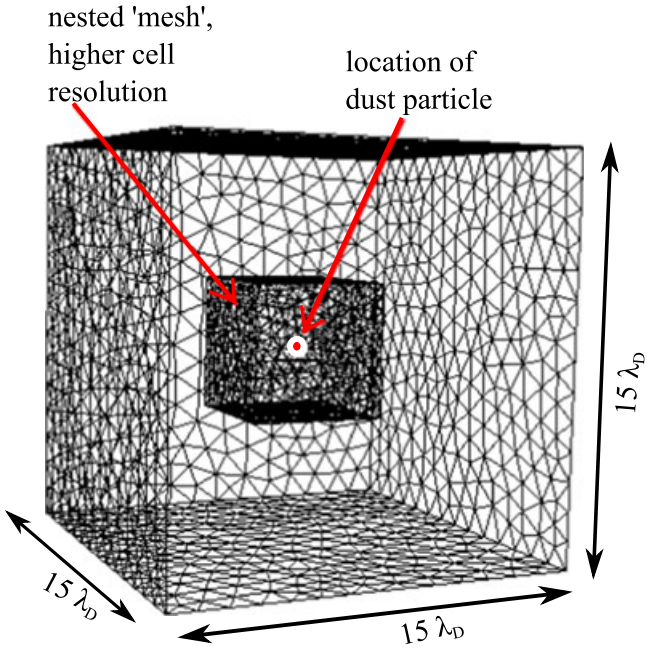

Figure 3. Simulation volume used in the single dust charging. The mesh is constructed with a large cell at the boundary and smaller cell toward the center of the volume, as shown by the surface mesh. At the location where the dust particle is placed, a finer mesh is employed to provide better resolution of the field, whereas at the boundary, a much larger mesh is used to assist plasma species sampling process. The top half contains the "dummy" probe and is not significant to the simulation as the "dummy" probe's surface potential is kept at 0 V. A single dust particle is introduced randomly close to the center of the small "cube" labeled A. Dust cloud is introduced inside the same "cube" labeled A, with dust superparticles' position randomly set at the beginning of the simulation.

is equal to the dust surface potential $\phi_d(t)$ given by *Whipple et al.* [1985] as

$$\phi_d(t) = \frac{Q_d(t)}{C} = \frac{Q_d(t)}{4\pi\varepsilon_0 r_d(1 + r_d/\lambda_D)}. \tag{14}$$

[17] The plasma particle also needs to overcome the repelling potential of the dust in order for a collision to occur, i.e.,

$$\left|1/2 m_s |v_s|^2 / q_s\right| > |\Delta\phi|. \tag{15}$$

Assuming a dust that is gaining negative surface potential, this condition ensures that an absorption collision can only take place if the electron's kinetic energy is larger than the dust potential energy. Particles with kinetic energy less than the dust's potential energy will simply be reflected or scattered. However, the reflection and the scattering process are not explicitly addressed by the simulation presented here.

[18] If the dust is in the form of a dust cloud ($a < \lambda_D$), competition for electrons/ions results in lower ϕ_d and the dust equilibrium charge number is reduced from the isolated case [*Goertz and Ip*, 1984; *Whipple et al.*, 1985]. In the following simulations, $r_d \ll \lambda_D$ is assumed and hence

$$\Delta\phi = \frac{Q_d(t)}{4\pi\varepsilon_0 r_d}. \tag{16}$$

[19] The conventional MCC algorithm which allows only one collision in every time step is reasonable if collision frequency between the two particles is small or constant. As dust particles can vary in size, each individual particle has its own collision rate and this has to be taken into account in determining the number of collisions that a dust particle is likely to experience in each time step. In addition, an uncharged dust particle at the beginning of a simulation can undergo multiple collisions in one time step compared to highly charged dust particle toward the end of the simulation as the collision cross section (σ_s) of the particle is highly dependent on the dust surface potential. The need for different collision frequency for each dust particle requires a different approach to the normal MCC algorithm. This is done by employing multistep MCC algorithm first proposed by *Gatsonis et al.* [1994]. In a multistep collision algorithm, the probability of a collision in a time step Δt is given by *Gatsonis et al.* [1994] as

$$P_1 = 1 - \exp\left[-\int_{T_L}^{T^{n+1}} \nu(t)\,dt\right] \tag{17}$$

where T_L is the time of the last collision, T^n is the time at the beginning of the time step Δt, and $T^{n+1} = T^n + \Delta t$. A uniform random number U_1 is then generated where

$$U_1 = 1 - \exp\left[-\int_{T_L}^{T_1} \nu(t)\,dt\right] \tag{18}$$

T_1 is the time for the particle to traverse the collision free path. Collision is assumed to happen if $P_1 > U_1$, which implies that $T_1 < T^{n+1} - T_L$, and T_L is then updated to T_1 ($T_L = T_1$). Multistep collision algorithm works by finding a new probability P_2 between the interval $T_L = T_1$ and T^{n+1}. A second uniform random number U_2 is generated for the same interval where the time T_2 is the time for the particle to travel before the next collision occurs. Collision happens if $P_2 > U_2$, which implies that $T_2 \le T^{n+1}$. The process is repeated until all collisions for a given time step are accounted for [*Gatsonis et al.*, 1994].

[20] The number of collision allowed over a time step Δt is given by

$$N_{as} = \nu_s \Delta_t \tag{19}$$

where collision frequency, ν_s, corresponds to the local (cell) parameters. These parameters include local density and particle speed in an area or volume where the dust is residing at its center. The dust and plasma superparticles are randomly paired such that actual collision depends on the possibility of the pair producing a collision. In the event of collision, particle charge (q_s) is added to the dust charge but the colliding plasma species superparticle loses K_d number of particles, where K_d is the dust superparticle weight which reflects the number of actual collisions that happened during that time step. In other words, every collision between plasma species superparticle and dust superparticle with weight K_s and K_d, respectively, represents K_d number of collisions and therefore require removal of K_d particles from K_s.

2.2. SPIS-Dust Code Development

[21] SPIS-dust has been developed based on SPIS software with the aim to simulate dusty plasma environment. It involves simulating plasma particles either in fluid form or using PIC technique. In the PIC implementation, dust

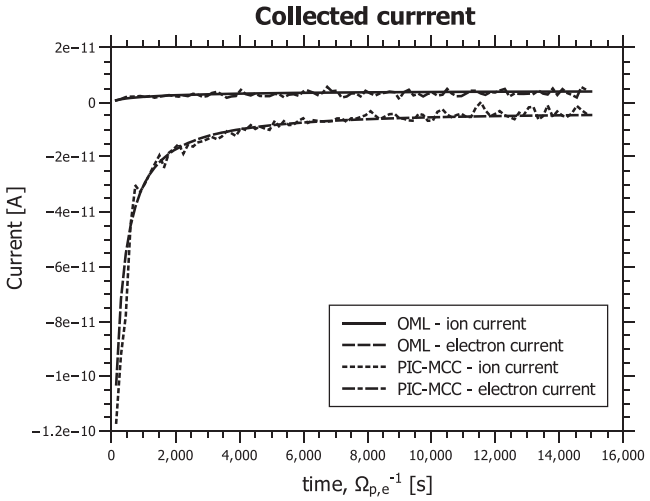

Figure 4. Current collection by the single dust grain shows almost identical result to the OML approximation. The OML currents are given as follows: ion (solid line) and electron (dashed), while the PIC-MCC simulation results are given as follows: ion (dotted line) and electron (dash-dotted).

particles are introduced as another plasma species. Rather than having fixed properties like any other fundamental species, dust particles' properties such as mass, size, and initial charge number can be varied according to user's requirement or the dusty plasma environment. These parameters can either be set to be uniform for all dust particles or follow a certain distribution function. The MCC algorithm is introduced in the code by an interaction routine that checks for possible collision between dust particles and the local plasma species based on techniques described in the preceding section.

[22] In a conventionally "structured" PIC simulation where the cells are equally sized, a correct choice of numerical parameters such as time step (Δt), cell size (Δx), and superparticle number per Debye length volume (N_d) is as important as the physical model and properties. Commonly accepted values for Δt and Δx as suggested by *Birdsall* [1991] and *Hockney and Eastwood* [1988] are

$$\omega_p \Delta t \lesssim 0.2 \tag{20}$$

$$\frac{\lambda_D}{\Delta x} \gtrsim 2. \tag{21}$$

Since the code employs unstructured mesh in constructing the cells, one immediate issue is the representation of plasma superparticles in every cells. Assuming plasma particles are represented by superparticles of weight K_s, variation in cell's volume results in unequal number of superparticles between the small and large cells. MCC technique requires a certain number of plasma particles in order not to lose the accuracy of the simulation [*Birdsall*, 1991]. As a result, a "dust-centered" cell is specified for the MCC where the cell's radius is determined by the number of dust particles required in each cell given by

$$N_{d,r_s} = \frac{4}{3}\pi r_s^3 \frac{n_s}{K_d} \tag{22}$$

where r_s is the cell's radius for the MCC sample. An unstructured mesh allows both low and high spatial resolution to be used in the simulation domain which could result in unbalanced number of superparticles per cell.

3. Results and Discussion

3.1. SPIS-Dust Code Validations

[23] The code is validated for two different scenarios to investigate its performance against well established theories. In the first scenario, a single dust particle is immersed in a dense ionospheric plasma and the dust charging process via the PIC-MCC technique is monitored. The result is compared to the solution obtained using the OML theory [*Mott-Smith and Langmuir*, 1926] which has been shown to provide good approximation of the current collected by a surface in space. In a case where secondary emission and photoemission are negligible, OML gives good approximation for the collected current [*Whipple*, 1981; *Fortov et al.*, 2005]. The next scenario involves charging of a cloud of dust particles in the ionospheric plasma environment. In this scenario, a finite size dust cloud with three different densities are placed in the plasma and the response of the PIC-MCC algorithm for each density is recorded. The results for the simulations are compared to the theoretical work by *Havnes et al.* [1990].

3.1.1. Single Dust Charging

[24] For single dust charging, simulation volume is set to $15\lambda_D \times 15\lambda_D \times 15\lambda_D$ m^{-3}, where $\lambda_D = 1.05 \times 10^{-2}$ m is the plasma Debye length. Dust particle is uncharged at the beginning of the simulation with $r_d = 100\,\mu$m and $Z_d = 0$ and is positioned at the center of the simulation volume as shown in Figure 3. The dust charging process is simulated for a typical ionospheric plasma with a Maxwellian distributions of electrons and singly charged oxygen O^+ ions.

[25] Ionospheric plasma, with densities $n_e = n_i = 10^{11}$ m^{-3} and temperatures $T_e = 0.2$ eV and $T_i = 0.1$ eV, is chosen for this validation purpose. Time step for the simulation is set to

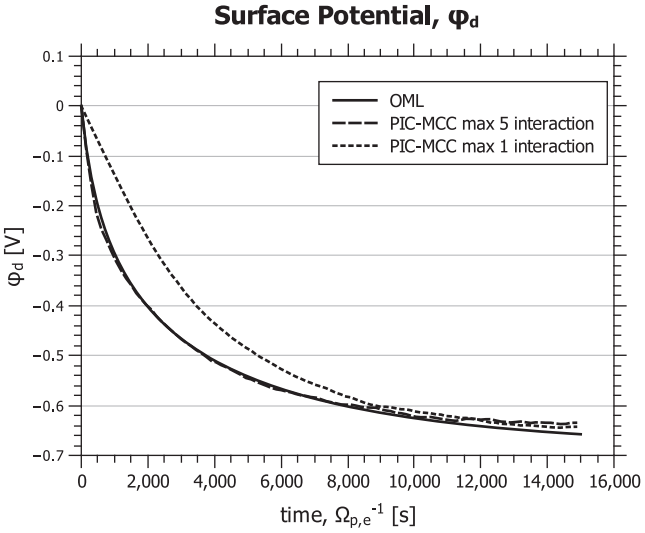

Figure 5. Dust particle surface potential compared to potential from OML approximation (solid). Up to five collisions are allowed in every Δ_t (dashed) and only one collision is allowed (dotted).

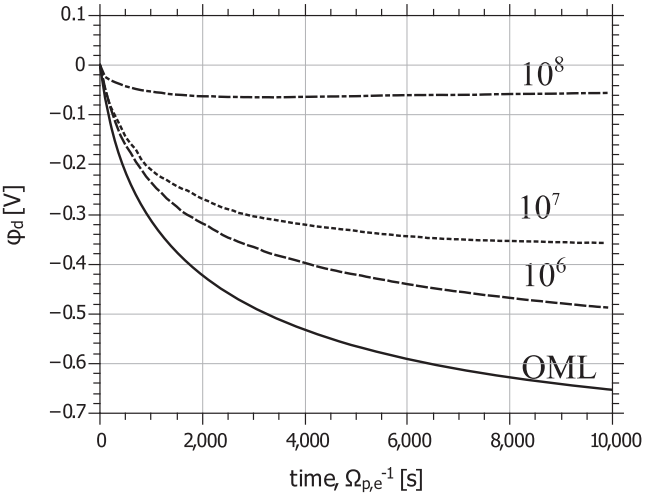

Figure 6. Average dust potential versus time in unit of plasma frequency (Ω_e^{-1}) for different dust cloud densities. The graph shows decreasing dust potential for increasing dust cloud density.

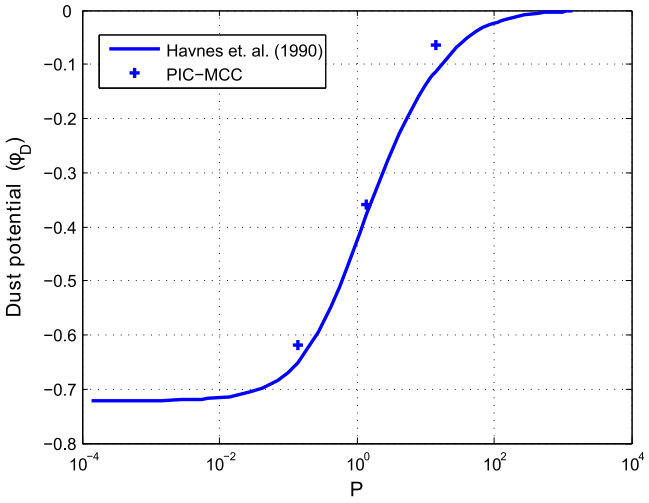

Figure 7. Average dust potential (plus marks) compared to the analytical solution by *Havnes et al.* [1990] (solid line) as a function of P.

$\Delta t = 0.1\Omega_{p,e}^{-1} = 5.6 \times 10^{-9} s$, and the simulation is performed for over $15,000\Omega_{p,e}^{-1}$ s. For the MCC, the interaction cell radius $r_s = 0.5\lambda_D$ and plasma particle weight, $K_s = 20,000$.

[26] Current collection by the dust particle is shown in Figure 4 for both ion and electron, which is compared to the solution provided by the OML theory. The multistep MCC employed appears to give good approximation of both electron and ion current especially during the initial dust charging phase. During the early stage of dust charging, electron current is at least an order of magnitude bigger than ion current, due to electrons having higher thermal energy than ions. On the numerical implementation, the higher electron current translates to high number of collision in each time step. In contrast, OML does not consider the charge discreetness when solving the current equations (3) and (4), and this could explain the charge fluctuation observed in the graph. In the simulation, the maximum number of collisions allowed for the PIC-MCC over a time step in the ionospheric environment is calculated using (19) for average particle velocity, i.e., $N_{as} = \nu_s \Delta t = 5.6 \sim 5$.

[27] Toward the end of the simulation, electron current can be observed to fluctuate at higher amplitude than ion current. These fluctuations can be explained by looking at the dust surface potential as shown in Figure 5. Figure 5

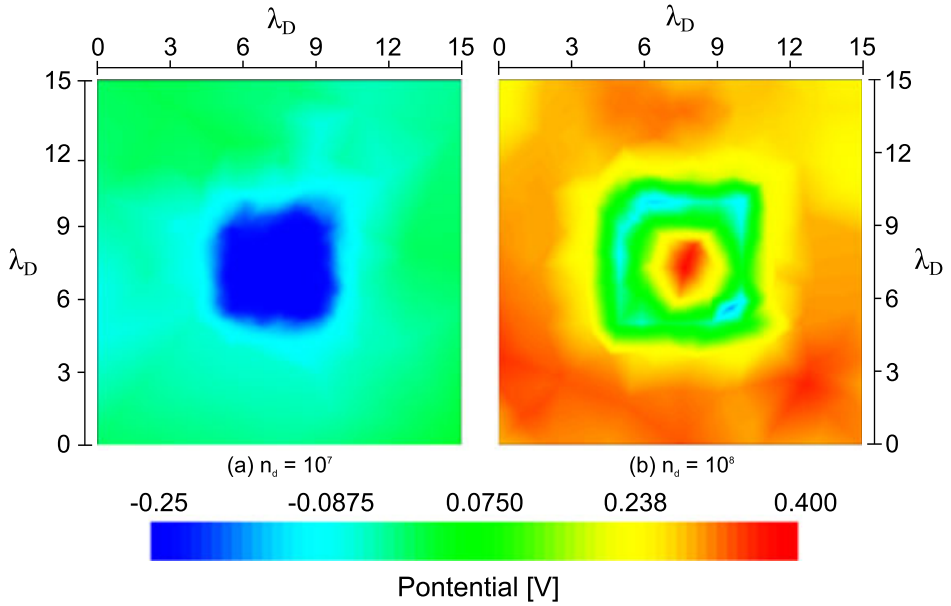

Figure 8. Plasma potential on the $x - z$ plane at $y = 0$ for dust cloud with (a) $n_d = 10^7$ m^{-3} and (b) $n_d = 10^8$ m^{-3}. The scale is in $\lambda/2$ with the snapshot taken at $t = 10,000\ \Omega_e^{-1}$. In Figure 8a, a homogeneous negative plasma potential is observed at the dust cloud position while in Figure 8b, the center of the cloud is positively charged due to screening effects caused by dust particle located at the edge of the cloud.

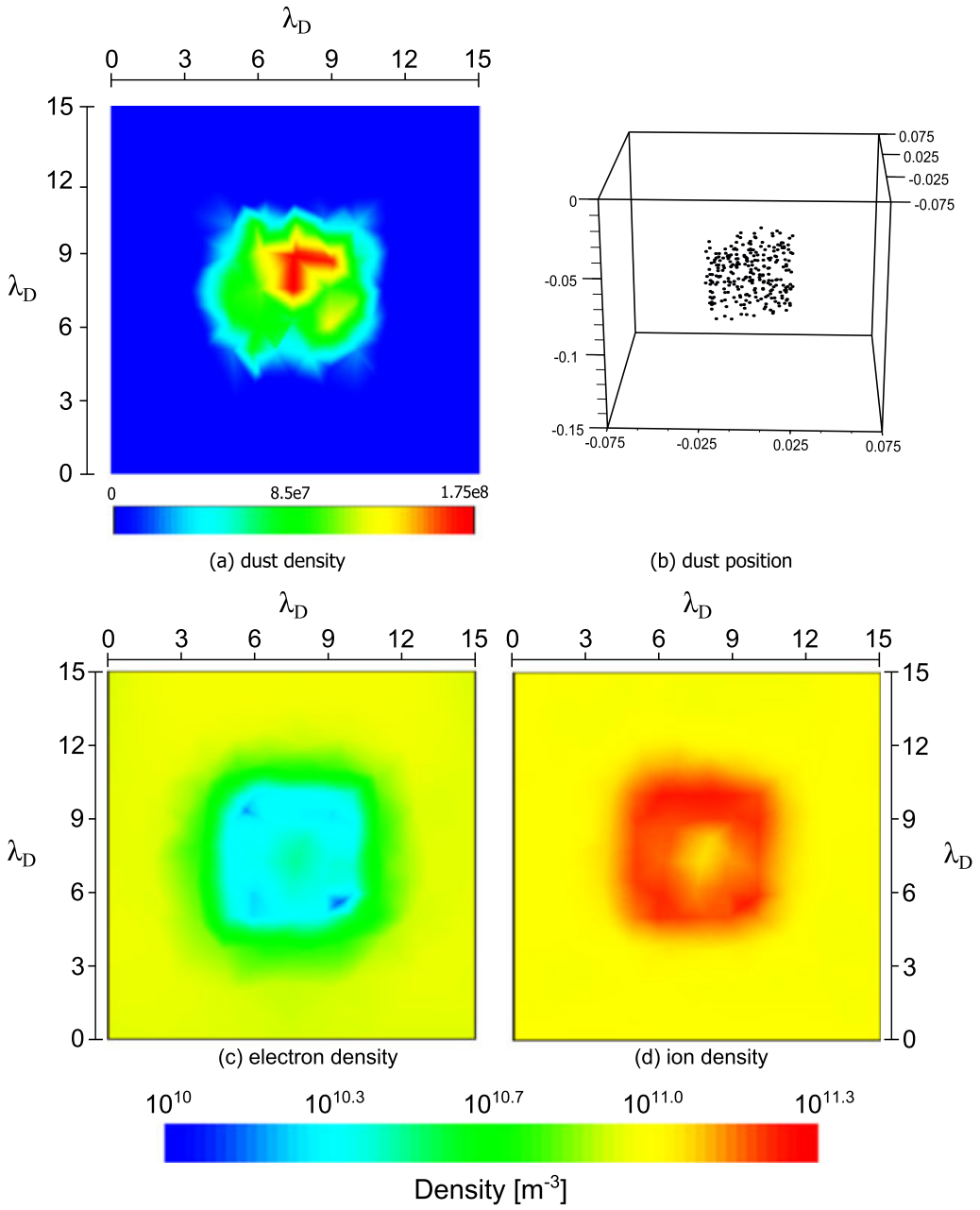

Figure 9. Plasma and dust density on the x–z plane at $y = 0$ for dust cloud with $n_d = 10^8\,\mathrm{m}^{-3}$. The scale is in λ_D with the snapshot taken at $t = 10,000\Omega_e$. (a) The dust cloud density and (b) the actual dust particles position in the cloud. The (c) electron and (d) ion density for the case of $N_d = 10^8$(c). In Figure 9c, a depleted electron region is clearly seen at the center of the cloud with density around 1/10 of the ambient electron density. In Figure 9d, increase in ion density around the cloud with twice the ambient density is observed at the cloud edges. This is caused by the attraction from negatively charged dust particles located at the cloud edges as compared to the center of the dust cloud where dust particles are positively charged.

shows the surface potential of the dust particle (dashed line) at plasma drift speed, $V_d = 0$ as a function of time using the PIC-MCC method in comparison with the one obtained from OML charging equation (solid line). As the magnitude of the dust potential increases, electrons are finding it harder to reach the surface due to the repulsive force generated by the surface. In the simulation, this results in underestimation of the dust charging rate which is caused by the random sampling process in the MCC. The fluctuations are found to cause less electrons from being collected by the surface and the dust surface is observed to charge to slightly lower magnitude than the OML approximation, with potential difference of less than 5% observed. Otherwise, the graph suggests good agreement between the theory (OML) and the simulation.

[28] Figure 5 also shows the PIC-MCC result (solid line) for dust charging process when there is only one collision per time step (dotted line). The charging curve for this case

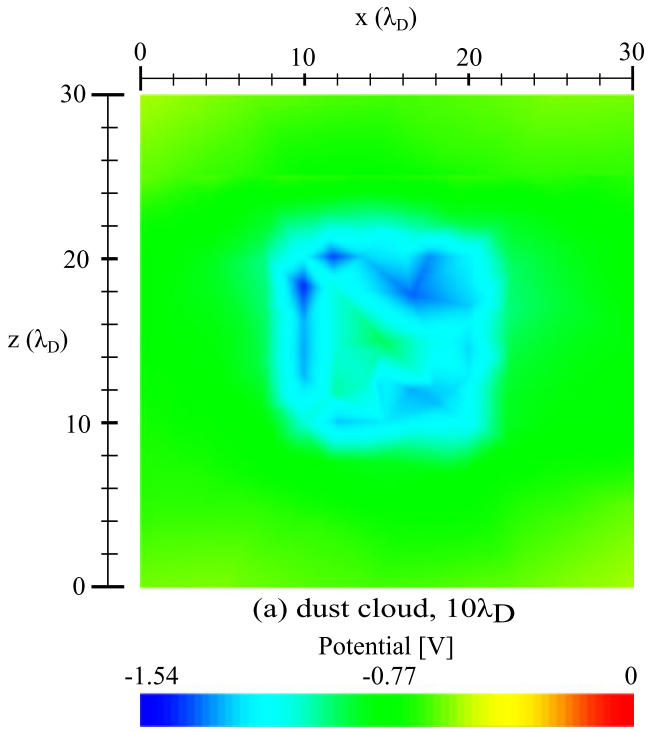

Figure 10. The 2-D view of the plasma potential surrounding a dust cloud with radius $10\lambda_D$ at $t = 10,000\ \Omega_e^{-1}$. A similar ring structure can be seen, although the potential of both the outer edge and inner side is negative. The dust cloud requires a much longer simulation period for it to have a similar potential level as in Figure 8.

indicates a significant underestimate of the rate of the dust charging process when compared to the OML hence justifying the need for multiple collisions, in particular for the dust radius presented here. For a particle with smaller radius, the effect of limiting the number of collisions for each time step will only prevail if $N_{as} > 1$, which is possible if the particle is positively charged.

3.1.2. Dust Cloud Charging in Unbounded Plasma

[29] It has been shown that increase in dust density causes the dust equilibrium charge to reduce significantly because of the dust collective effect [*Whipple et al.*, 1985]. This is a direct result from the neutrality condition, i.e.,

$$\frac{n_e}{n_i} = 1 - Z_d \frac{n_d}{n_i} \tag{23}$$

In (23), the term $Z_d \frac{n_d}{n_i}$ can be used to determine whether the dust particle in the plasma system is in isolation or not. If $Z_d \frac{n_d}{n_i} \ll 1$, the dust particle is isolated and when it is comparable to 1 ($Z_d \frac{n_d}{n_i} \rightarrow 1$), the dust particles are no longer isolated. This equation also shows that increase in n_d results in decreasing Z_d, because there are more dust particles competing for the same number of electrons, in other words, number of available electron per dust grain decreases. In these simulations, finite cloud of uncharged dust with dimension of $5\lambda_D \times 5\lambda_D \times 5\lambda_D$ is introduced at the beginning of the simulation in a simulation volume of $15\lambda_D \times 15\lambda_D \times 15\lambda_D$. The plasma is taken to be a typical ionospheric plasma with Maxwellian distribution, i.e., $n_e = n_i = 10^{11}$ m^{-3}, $T_e = T_i = 0.2$eV. Ions are singly charged oxygen O^+, which is the usual constituent for this type of plasma. The dust particles have a uniform radius of 100 μm and the mass density of individual particles are 3000 kg m^{-3} and are randomly placed in the dust cloud. The density of the cloud is varied for three different concentrations with $n_d = 10^6, 10^7$, and 10^8 m^{-3} with the dust superparticle weight of 1, 10, and 50 producing 124, 133, and 254 dust superparticles, respectively, in the $5\lambda_D \times 5\lambda_D \times 5\lambda_D$ cloud. Each plasma superparticle represents 20,000 real particles and simulation began with the loading of approximately 31,000 particle for each species. At every time step, new particles are injected into the simulation volume from each six boundary plane, and particles leaving the simulation volume are discarded. Dust charging for all three different dust cloud densities are simulated for a period of $10,000\Omega^{-1}$s, and the resulting dust potential is plotted in Figure 6 as a function of time. For comparison, dust potential for a single dust particle is included in the same graph.

[30] The average dust charge is calculated as $\overline{Q_d} = \sum_{i=1}^{N_d} Q_{d,i}/N_d$, where $Q_{d,i}$ is the number of charge on the ith dust superparticle and N_d is the total number of particles in the dust cloud. The dust potential $\overline{\phi_D}$ is calculated using the relation $Q_d = 4\pi\varepsilon_0 r_d \phi_D$, where ϕ_D is the relative potential difference between the dust and the plasma following the method in *Havnes et al.* [1990]. The average presented here refers to the average potential for each individual grain in the cloud with respect to plasma potential at a distance far away from the cloud (0 V). The graph in Figure 6 suggests that increase in dust cloud density will result in smaller Z_d, as indicated by the reduction in the magnitude of $\overline{\phi_D}$. Another observation that can be made from the graph is that the higher-density dust cloud achieves equilibrium state faster than the lower-density cloud. The equilibrium potentials depicted in the graph do not mean that current of each of the particles in the cloud is balanced, but an indication that the total current collected by the cloud is balanced.

[31] Another important technique in determining the dust cloud collective behavior is explained by the P parameter given by equation (6) [*Havnes et al.*, 1987, 1990]. For

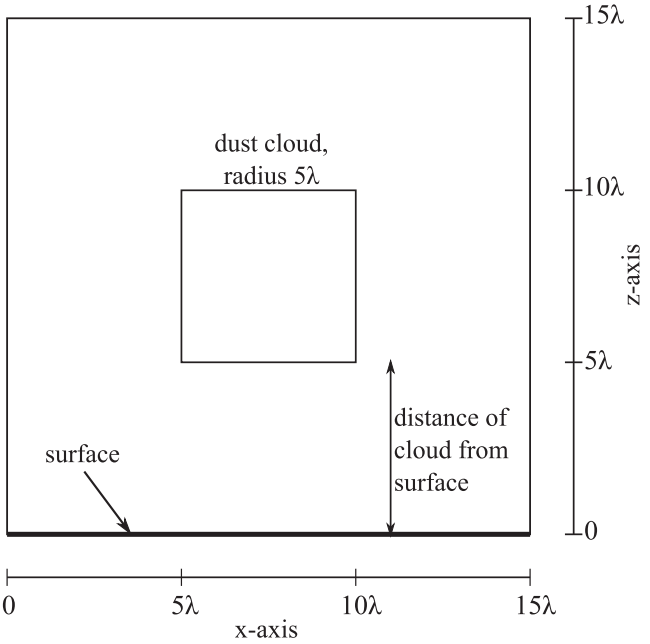

Figure 11. The 2-D view of the simulation model.

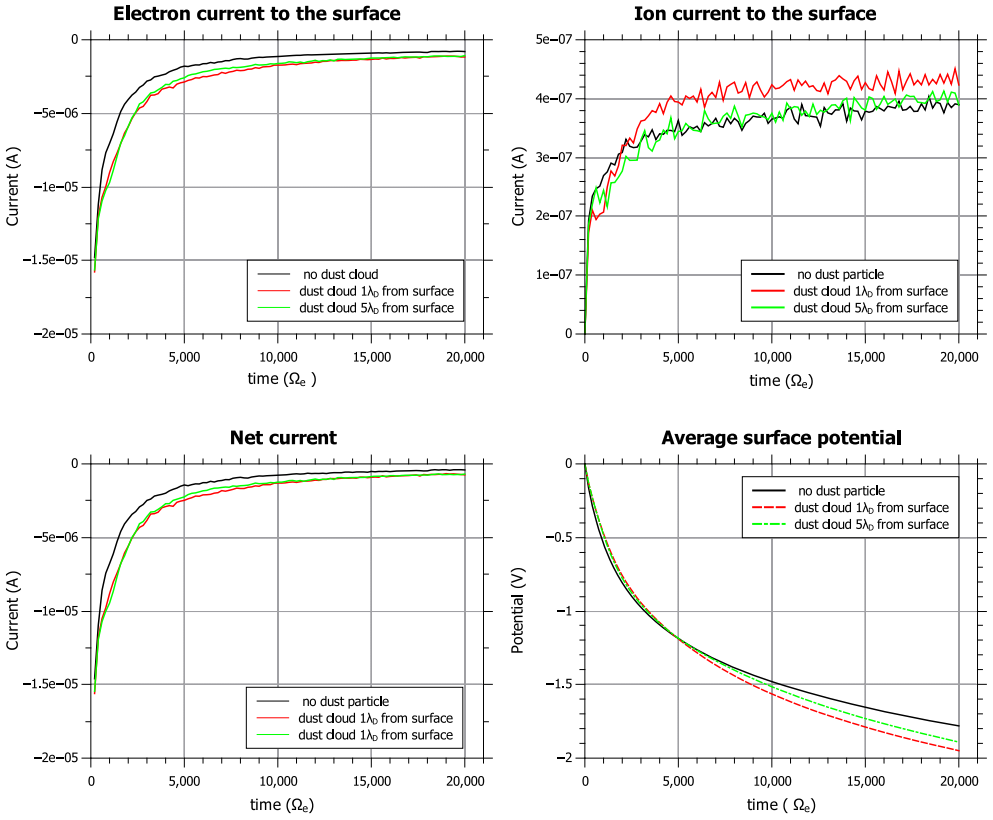

Figure 12. Current collection and surface potential for the three cases: no dust cloud (black), dust cloud $1\lambda_D$ from the surface (red), and dust cloud $5\lambda_D$ from the surface. Increase in (a) electron and (b) ion current for both cases of dust cloud. The increase in ion current however is higher for the case where the cloud is much closer to the surface. (c)The net current coming onto the surface and (d) the average surface potential where the dust cloud is observed to have caused the potential to decrease further.

ionospheric plasma with electrons and singly charged oxygen ions, P is evaluated for the three dust's densities which are 10^6 m^{-3}, 10^7 m^{-3}, and 10^8 m^{-3}, giving P values of 0.139, 1.39, and 13.9, respectively. The value of P can be used as an indication of increasing dust collective effect on dust charging. Figure 7 shows $\overline{\phi_D}$ versus P. The graph compares the results obtained from the simulations with the approximate rational functions for the evaluation of P provided by *Havnes et al.* [1990], which shows that the $\overline{\phi_D}$ for the three values of P obtained from the simulation are in good agreement, although a slightly lower average is observed for $n_d = 10^8$m^{-3}. Similar results were observed by *Gatsonis et al.* [1994], and it was argued that the difference was due to the fact that *Havnes et al.* [1990] did not include the effect of nonthermalized plasma in the derivation of their solution.

[32] Figure 8 compares the cross section of the dust cloud potential for finite dust clouds with densities of 10^7 m^{-3} and 10^8m^{-3}, as obtained from the simulation. Observation of the dust particle dynamics indicates negligible dust motion due to the small simulation period. In Figure 8a, simulation suggests a slight perturbation in plasma potential around the edges of the negatively charged cloud. In Figure 8b, simulation indicates the formation of a negative ring structure, around a region of positive plasma potential. Assuming that the plasma potentials observed in both figures are due to the presence of charged dust particles, a conclusion can be made for the cases of dust cloud with different P values. For $P \sim 1$, particles in the cloud are charged to around the same Q_d, whereas for $P > 10$, particles located on the edge are negatively charged while the one inside the cloud are positively charged.

[33] Figures 9a and 9b show the dust density and the dust particles position in the cloud, respectively, while Figures 9c and 9d show the electron and ion density for the case of $N_d = 10^8$, respectively. In Figure 9c, a depleted electron region can be observed in the dust cloud with maximum depletion appearing at the edge of the cloud. In contrast, Figure 9d indicates that ion density at the edge of the cloud is $\sim$ 1.5 times higher than the ambient ion density. Inside the cloud, ion density is found to be equal to the ambient density, similar to the observation in *Goertz et al.* [2011]. These two figures suggest electron retardation and ion attraction regions at the dust cloud edge. In addition, ions are found to be in higher density than electrons in the middle of the dust cloud. These results are in good agreement with the observation made by *Gatsonis et al.* [1994], although the boundary between the neutral and the disturbed plasma is not visible in the figures due to the small simulation volume.

[34] Adding to the observation of plasma potential in Figure 8b, the following scenarios are envisaged. The edge of dust cloud is getting charged largely by electrons (due to higher thermal speed) which develops negative potential region. This creates the negatively charged dust layer that repels incoming electrons, creating a depleted electron

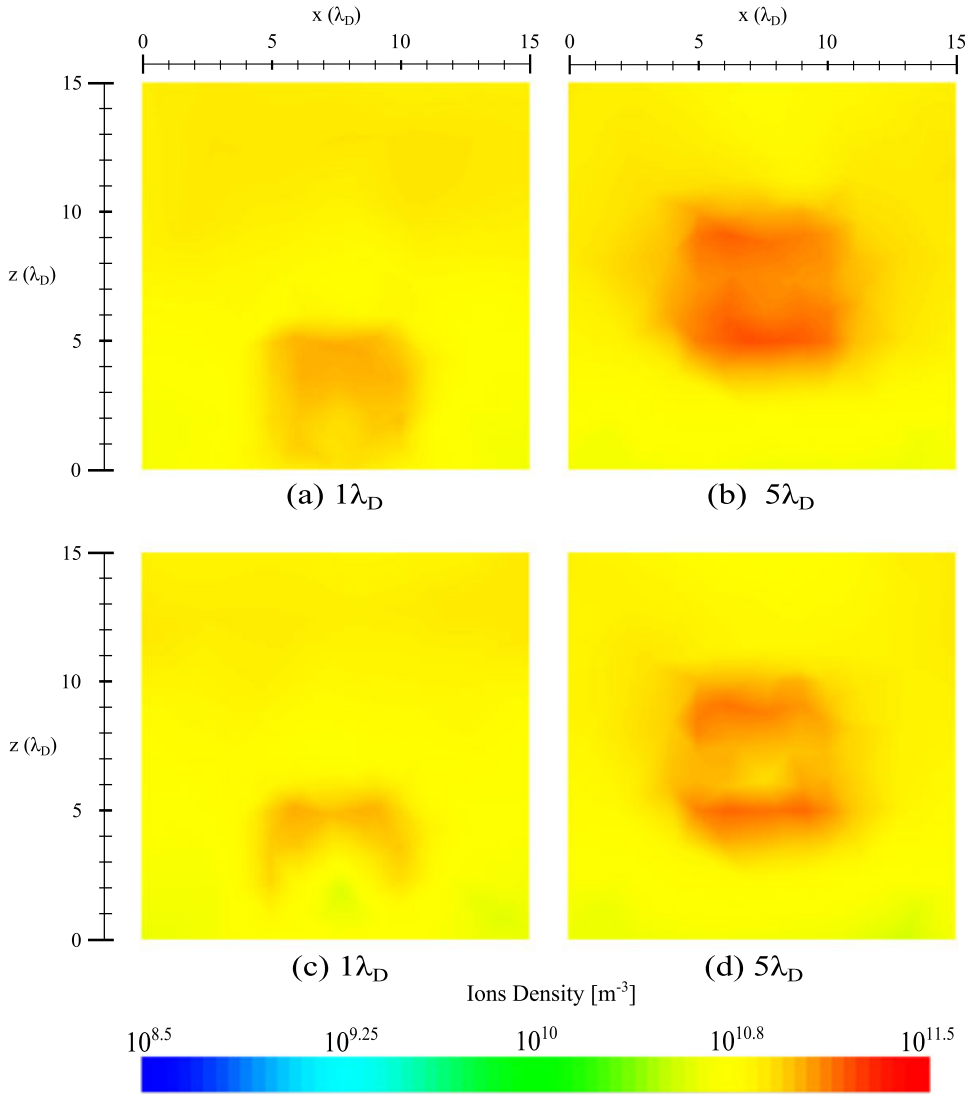

Figure 13. Ion density on the $x - z$ plane at $y = 0$ for dust cloud with $n_d = 10^8$ m^{-3}. The scale is in λ_D with the snapshot taken at (a and b) $t = 10,000\ \Omega_e^{-1}$, and at (c and d) $t = 20,000\ \Omega_e^{-1}$. In Figures 13a and 13b, a high concentration of ions are observed on both dust cloud, and in Figure 13c, high ion density is observed only on the top edge of the cloud which is further away from the charged surface, while in Figure 13d, high ion density can be seen forming a ring around the cloud edge. In Figure 13c, ions are attracted to the negative potential on the surface, leaving an area depleted of ions.

region in the middle of the cloud and at the same time accelerates incoming ions that form the concentrated ion region at the edge of the cloud. Electrons that are able to pass through the negative dust layer appear to be slowed down in the middle of the cloud, as indicated by the slight increase in electron density in the middle of the cloud. On the other hand, ions passing through the dust cloud are dragged toward the edge leaving a depleted ion region inside the cloud. In the middle of the cloud, depleted electrons reduce the number of electron-dust collision. Ions, although moving slower than electrons, are present in large numbers in the middle of the dust cloud. This increases the chance of ion-dust collisions, resulting in positively charged dust particles.

[35] To investigate whether the observations of the potential ring structure is dependent on the size of the dust cloud, another simulation has been carried out where the radius of the dust cloud is set to double from $5\lambda_D$ to $10\lambda_D$, and the density is maintained at 10^8m^{-3}. The system is simulated for a period of $10,000\Omega_e$ and the resulting dust cloud and plasma potential is shown in Figure 10. The plot shows the development of similar potential structure around the dust cloud, where the outer edge of the cloud is more negatively charged compared to the inner cloud. This happens simply because the larger dust cloud requires a much longer time to reach equilibrium. Based on the results, it can be concluded that even though the development of the ring structure is time dependent, the formation of the potential well seems to be more depending on the dust cloud density rather than the size of the cloud. At low dust density ($P < 1$), each particle in the dust cloud behaves in a similar manner as a single dust particle, and the charging process can be approximated

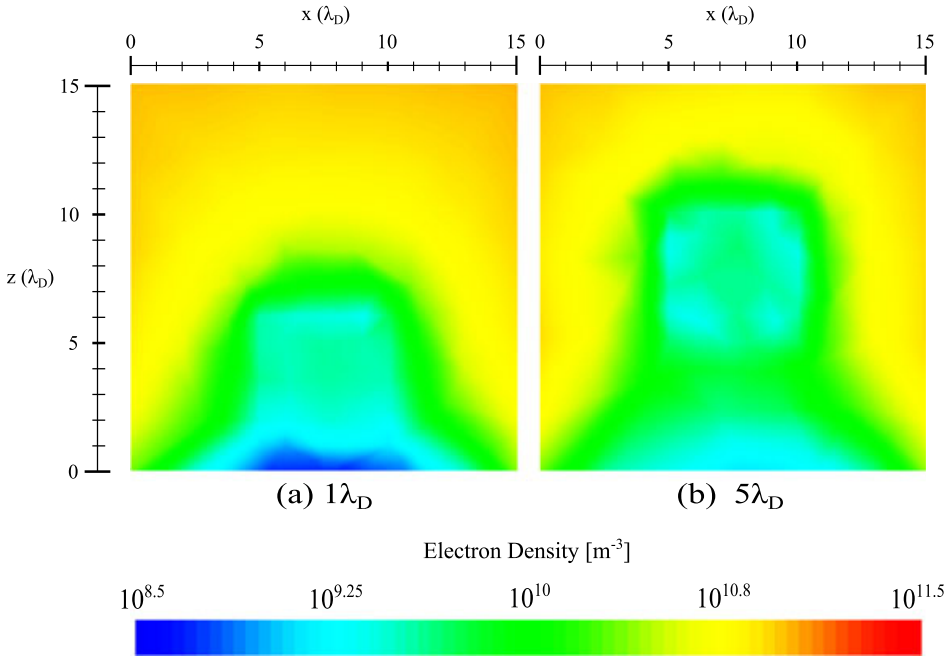

Figure 14. Electron density on the $x - z$ plane at $y = 0$ for dust cloud with $n_d = 10^8$ m^{-3}. The scale is in λ_D with the snapshot taken at $t = 20000\ \Omega_e^{-1}$. (a) Electron density between the cloud and the surface for the case where the distance in between them is $1\lambda_D$, which is an order of magnitude lower than the one where the dust cloud is located at (b) $5\lambda_D$. In both cases, the structure of the depletion region is similar to a wake region caused by objects in flowing plasma.

by the OML theory. However, when $P > 1$, the difference in electron and ion density around the dust cloud means that dust particles located at the edge are charged to negative potential while the ones in the middle of the cloud are positively charged.

3.2. Dust Cloud Near a Charged Surface

[36] A spacecraft in space releases dust particles into its surrounding environment which can affect spacecraft operations. These can be originated from trapped dust particles on spacecraft's surface or from spacecraft's operational tasks such as exhaust, thrusters firing, and liquid dump, hence, their size and radius vary depending on the source. In space, spacecraft's surfaces are charged to negative or positive potential depending on the net species flux, which in many ways are similar to the charging process experienced by a dust particle. Simulations reported in this section consider a surface which represents a spacecraft in an ionospheric plasma environment releasing a cloud of trapped dust particles into its surrounding. The surface is assumed to be conducting with initial potential of 0 V. No other surface interactions such as photoemission or secondary emission are included in the simulation. This condition is akin to the environment a spacecraft might encounter during its initial orbital injection.

[37] The dust particles have the same basic properties (size, mass, and cloud radius as in the previous simulations, and the particles are assumed to be uncharged at the beginning of the simulation. The dust cloud has a radius of $5\lambda_D$ with densities of $n_d = 10^8$ and is initialized at two different distances from the spacecraft, at $1\lambda_D$ and at $5\lambda_D$. Plasma particles are injected from the boundary planes, and each superparticles represents 20,000 actual particles, as in the previous section. The 2-D view of the simulation model is shown in Figure 11.

[38] The surface's current collections and surface potential are shown in Figure 12. In Figure 12a, there is an increase in electron current for the two different cases of dust clouds when compared to the one without the dust cloud. There is, however, a slight increase in ion current when the dust cloud is closer to the charged surface. The increase in ion current is an order of magnitude smaller than the electron current, making its contribution to the total net current almost insignificant as shown in Figure 12c. This results in slightly higher negative potential on the surface when compared to the case with no dust particle as in Figure 12d.

[39] As the spacecraft surface is charged to negative potential, ions are accelerated toward the surface. The presence of dust cloud increases this attracting force, with the dust cloud closer to the surface contributing more to the attracting force than the one that is further away. This is clearly illustrated in Figure 13. Figures 13a and 13c show ion densities for the cases where the dust cloud is $1\lambda_D$ from the surface while Figures 13b and 13d show the ion densities when the dust cloud is located $5\lambda_D$ from the surface. The first two figures are taken at $t = 10,000\Omega_e$s while the latter two are taken at the end of the simulation at $t = 20,000\Omega_e$s. Halfway through the simulation at $t = 10,000\Omega_e$s, a high ion concentration can be seen in both dust clouds (Figures 13a and 13b). Ions that were previously trapped inside the dust cloud have moved toward the surface, where they are collected. As a result, for the cloud that is close to the surface, a region of depleted ions appears at the bottom edge of the cloud (Figure 13c).

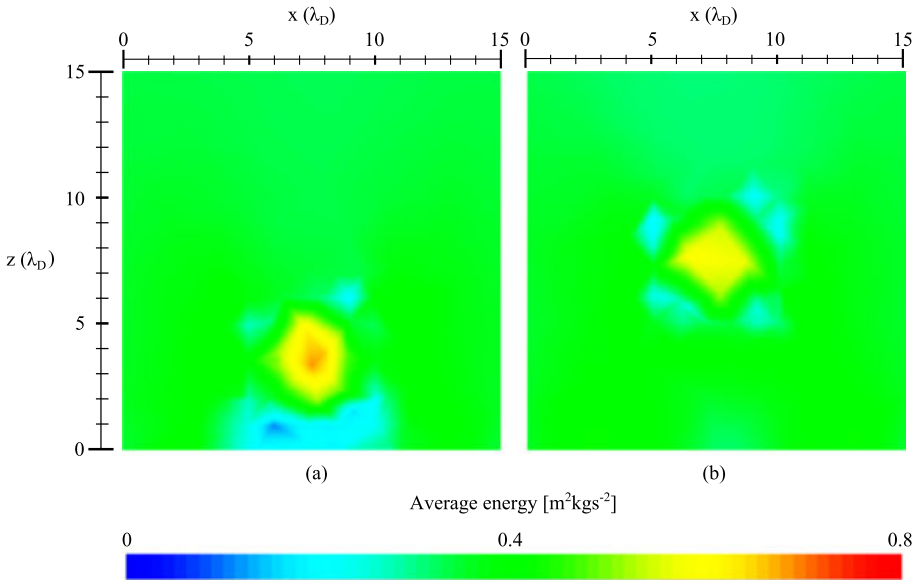

Figure 15. Electron energy map on the $x-z$ plane at $y = 0$ for a dust cloud with $n_d = 10^8$ m^{-3} located at a distance of (a) $1\lambda_D$ and $5\lambda_D$ from the surface. The scale is in λ_D with the snapshot taken at $t = 20,000\,\Omega_e^{-1}$. In Figure 15a, higher-energy electrons can be found in the middle of the cloud because of the potential barrier created by both the surface and the dust cloud that repels the low-energy ones. Also visible is the region of low-energy electrons trapped between the cloud and the surface. These electrons have less energy to overcome the surface and the dust cloud potential barrier. In Figure 15b, high-energy electrons can be observed in the middle of the dust cloud with low-energy ones that appear to have been repelled by the dust cloud potential barrier.

[40] The presence of a charged surface also creates a region of depleted electrons. Electrons are being repelled from the surface, and the effect is significant when the cloud is close to the surface. In Figure 14a, electron density between the dust cloud and the surface is an order of magnitude lower than the one where the cloud is located at a distance of $5\lambda_d$ from the surface as in Figure 14b. The structure of the electron depleted regions is similar to a wake region often encountered when an object passes through a streaming plasma. Simulations also reveal that electrons inside both dust clouds are made of high-energy electrons as illustrated in Figure 15, with more energetic electrons observed on the cloud closer to the surface. In both cases, low-energy electrons appear to have been repelled by the cloud, creating a layer around the dust cloud. In addition, Figure 15a indicates that there is a region where low-energy electrons are trapped between the dust cloud and the negatively charged surface as these electrons have less energy to overcome the potential barrier created by the surface and the dust cloud.

4. Summary and Conclusion

[41] The results presented show the potential of using a publicly available unstructured three-dimensional plasma simulation software to study the dust charging process by employing PIC-MCC into the code. In order for the dust charging process to be adequately modeled, a multistep MCC has been employed in order to cater for the variation in dust charging rate. In the isolated dust scenario, the charging process simulated using the multistep MCC algorithm is in good agreement with the analytic solution provided by the OML theory. The dust particle has been shown to charge to approximately the same rate as in OML, albeit for some current fluctuations toward the end of the simulation which cause an underestimate of the dust potential. This under estimation of the charging process is more likely to be caused by missing collisions due to the dust particle reaching its saturation dust charge number.

[42] The multistep MCC technique implemented in this work also provides a good approximation to the dust cloud scenario where the average equilibrium dust charge falls within the range of the analytical solution. In the dust cloud simulation, the effect of dust density to the dust cloud potential and its surrounding plasma has been presented which indicates the formation of ring-like structure on the dust cloud for $n_d = 10^8$ m^{-3}. This ring-like structure is caused by plasma neutrality being violated as the outer dust particle creates a potential barrier when charged. This barrier prevents low-energy electrons from reaching the inner cloud and at the same time attracts ions. As a result, a positive plasma potential is observed at a distance of more than $5\lambda_D$ from the dust cloud as well as in the inner cloud itself.

[43] In assessing the spacecraft charging in the presence of dust particles, simulations were carried out for two cases where (a) the dust was positioned at $1\lambda_D$ with respect to the spacecraft surface and (b) where the distance of dust cloud and the surface was kept at $5\lambda_D$. The simulation revealed that the spacecraft's surface was charged to a higher negative potential due to increase in electron current. Once negative potential is developed on the spacecraft's surface, ions become attracted causing the ring structure to disappear. This effect is more pronounced when the dust cloud is closer to the surface. In addition, the dust cloud creates

regions of low- and high-energy electrons and in one case, with low-energy electrons being trapped between the dust cloud and the charged surface. This indicates that a cloud of dust particles, when released from a spacecraft surface, can affect electron and ion collection, resulting in a lower surface potential. Although the simulation performed can be attributed to a worst case scenario, where the maximum size of dust particles are released into space, the simulation results illustrate the importance of dust contamination when designing any space bound vehicle.

[44] **Acknowledgments.** The authors would like to express their gratitude to the European Space Agency (ESA), the SPIS team at ONERA and the Ministry for Higher Education, Malaysia for supporting this study.

[45] Philippa Browning thanks the reviewers for their assistance in evaluating this paper.

References

Birdsall, C. K. (1991), Particle-in-cell charged-particle simulations, plus Monte Carlo collisions with neutral atoms, PIC-MCC, *IEEE Trans. Plasma Sci.*, *19*(2), 65–85.

Brieda, L., A. Barrie, D. Hughes, and T. Errigo (2010), Analysis of particulate contamination during launch of the MMS mission, in *Proceedings of SPIE 7794, Optical System Contamination: Effects, Measurements, and Control, The International Society for Optical Engineering,* vol. 7794, SPIE, Bellingham, Wash.

Cui, C., and J. Goree (1994), Fluctuations of the charge on a dust grain in a plasma, *IEEE Trans. Plasma Sci.*, *22*(2), 151–158.

Fortov, V. E., A. V. Ivlev, S. A. Khrapak, A. G. Khrapak, and G. E. Morfill (2005), Complex (dusty) plasmas: Current status, open issues, perspectives, *Phys. Rep.*, *421*, 1–103.

Gatsonis, N. A., R. E. Erlandson, and C.-I. Meng (1994), Simulation of dusty plasmas near surfaces in space, *J. Geophys. Res.*, *99*(A5), 8479–8489.

Goertz, C. K. (1989), Dusty plasmas in the solar system, *Rev. Geophys.*, *11*(4), 271–292.

Goertz, C. K., and W.-H. Ip (1984), Limitation of electrostatic charging of dust particles in a plasma, *Geophys. Res. Lett.*, *11*(4), 349–352.

Goertz, I., F. Greiner, and A. Piel (2011), Effects of charge depletion in dusty plasmas, *Phys. Plasmas*, *18*, 013703.

Goree, J., and Y. T. Chiu (1993), Dust contamination of the spacecraft environment by exposure to plasma, *J. Spacecraft Rockets*, *30*, 765–766.

Goree, J. (1994), Charging of particles in a plasma, *Plasma Sources Sci. Technol.*, *3*, 400–406.

Havnes, O., C. K. Goertz, G. E. Morfill, E. Grün, and W. Ip (1987), Dust charges, cloud potential, and instabilities in a dust cloud embedded in a plasma, *J. Geophys. Res.*, *92*, 2281–2287.

Havnes, O., T. K. Aanesen, and F. Melandsø (1990), On dust charges and plasma potentials in a dusty plasma with dust size distribution, *J. Geophys. Res.*, *95*, 6581–6585.

Hilgers, A., S. Clucas, B. Thiebault, J.-F. Roussel, J.-C. Mateo-Velez, J. Forest, and D. Rodgers (2008), Modeling of plasma probe interactions with a PIC code using an unstructured mesh, *IEEE Trans. Plasma Sci.*, *36*(5), 2319–2323.

Hockney, R. W., and J. W. Eastwood (1988), *Computer Simulation Using Particles*, Adam Hilger, London, U. K.

Jana, M. R., A. Sen, and P. K. Kaw (1993), Collective effects due to charge-fluctuation dynamics in a dusty plasma, *Phys. Rev. E*, *48*(5), 3930–3933.

Lapenta, G., and J. U. Brackbill (1997), Simulation of dust particle dynamics for electrode design in plasma discharges, *Plasma Sources Sci. Technol.*, *6*, 61.

Mendis, D. A. (1979), Dust in cosmic plasma environments, *Astrophys. Space Sci.*, *65*, 5–12.

Mott-Smith, H. M., and I. Langmuir (1926), The theory of collectors in gaseous discharges, *Phys. Rev.*, *28*(4), 727–763.

Murphy, D. L., and Y. T. Chiu (1991), Dusty plasmas in the vicinity of a large dielectric object in space, *J. Geophys. Res.*, *96*, 11,291–11,305.

Northrop, T. G. (1992), Dusty plasmas, *Phys. Scr.*, *45*(5), 475–490.

Robinson, P., P. Leung, J. Feynman, S. Gabriel, R. Wuerker, A. Wong, E. Seale, and O. Short (1991), Observation and impact of dust particles on the Magellan mission to Venus, in *Vehicle-Environment Interactions Conference,* vol. 155, edited by R. Erlandson and C. I. Meng, p. 155, Applied Physics Laboratory, The Johns Hopkins Univ., Laurel, Maryland.

Rovagnati, B., M. Davoudabadi, G. Lapenta, and F. Mashayek (2007), Effect of collisions on dust particle charging via particle-in-cell Monte-Carlo collision, *J. Appl. Phys.*, *102*, 073302-1–073302-9.

Roussel, J.-F., F. Rogier, G. Dufour, J.-C. Mateo-Velez, J. Forest, A. Hilgers, D. Rodgers, L. Girard, and D. Payan (2008), SPIS open-source code: Methods, capabilities, achievements, and prospects, *IEEE Trans. Plasma Sci.*, *36*(5), 2360–2368.

Shukla, P. K. (1994), Shielding of a slowly moving test charge in dusty plasmas, *Phys. Plasmas*, *1*(5), 1362–1363.

Shukla, P. K. (2001), A survey of dusty plasma physics, *Phys. Plasmas*, *8*, 1791–1803.

Spitzer, L. Jr. (1941), The dynamics of the interstellar medium. I. Local equilibrium, *Astrophys. J.*, *93*, 369–379.

Whipple, E. C. (1981), Potentials of surfaces in space, *Rep. Prog. Phys.*, *44*(11), 1197–1250.

Whipple, E. C., T. G. Northrop, and D. A. Mendis (1985), The electrostatics of a dusty plasma, *J. Geophys. Res.*, *90*, 7405–7413.